MANIPULATING ITO-BASED CONTROLLABLE PHASE SHIFTERS FOR DESIGNING A COMPACT, HIGH BANDWIDTH OPTICAL MODE SELECTIVE ROUTER INTEGRATED ON SILICON-ON-INSULATOR WAVEGUIDES

Duy Nguyen Thi Hang[*], Thuy Tran Thi Thanh[*], Tan Hung Nguyen[#], Cao Dung Truong*
[*]Posts and Telecommunications Institute of Technology of Vietnam;
[#]Advanced Institute of Science and Technology-The University of Danang

Abstract: Recently, Indium Tin Oxide, a highly transparent, well conductive, and CMOS-compatible material, has been paid strong attention to the thermo-optic controlled silicon photonics industry because it allows a miniature of the gap between the core silicon and the metallic heater, thus enabling reducing the electric power consumption and enhancing the switching speed. In this article, we propose an ultralow loss and small-size ITO microheater for the phase shift tuning. The designated microheater is manipulated to realize a numerical design of a compact and high bandwidth three-mode selective router. Simulation results illustrate the 3-dB bandwidth for the three-mode selective router as much as 100-nm and 40-nm with crosstalk under -25 dB, respectively. Besides, the designed device attains relatively large fabrication tolerances corresponding to width and height tolerances of ±50 nm and ±5 nm. In addition, the proposed devices consumed less than 90 mW total power consumption and took a fast switching time below 8 μs. Moreover, the design structure of the suggested mode selective router can be integrated into an estimated compact footprint of 8 μm×2160 μm. Such excellent performances demonstrate the attractive potential of ITO as low-loss thermo-optic phase shifters and open an alternative way for enabling ultrafast and high-speed mode division multiplexing systems and very large-scale photonic integrated circuits.

Keywords: ITO material; thermo-optic phase shifter; silicon-on-insulator; mode selective router; numerical simulation;

Contact author: Cao Dung Truong
Email: dungtc@ptit.edu.vn
Manuscript received: 25/6/2022, revised: 24/7/2022, accepted: 22/8/2022.

I. INTRODUCTION

Recently, in order to respond to the requirements of rapid capacity growth in optical networks, mode division multiplexing (MDM) has emerged as a promising solution to enhance the information transmission capacity and processing proficiency to overcome the Shannon limit [1–4]. It is widely considered that, in many technological platforms used to develop microchips components for the optical signal processing issue in general and mode division multiplexing technique in particular for optical communication networks, photonic integrated circuit (PIC) is one of the most preferred technological platforms. PICs have become prevailed technology because PIC can integrate various signal processing components in compact and flexible configurations. Nowadays, silicon-on-insulator (SOI) waveguide-based structures are prevalent for the realization of dense photonic integrated circuits and firmly established within the optoelectronic industry because they contain many advantages of low optical losses over the third telecom wavelength range, high confinement of light in small cross-section, reasonable manufacturing cost thanks to full compatibility with complementary metal-oxide-semiconductor technology [5].

Among essential components for optical mode processing, except for mode multiplexers/demultiplexers [6], [7], most of the mode signal processing components are related to the switching mechanism, such as mode converters [8], mode switches [9–11], mode routers . The switching function of optical signals in silicon photonic waveguides depends on the ability to control the phase of the optical field. The most common way to induce a dynamic phase shift is by exploiting the thermo-optic (TO) coefficient of the silicon core layer because of the sizeable thermo-optic coefficient ($\sim 1.8\times10^{-4}$ K^{-1}) [12] or exploiting the carrier effect by doping the conductor concentrations of group III/V elements [13], [14]. Although the carrier effect is capable of producing high-speed phase shifts and small

size integration, it suffers some drawbacks from the large optical loss and a relatively complex multi-layer fabrication process, thus leading to an expensive cost. Also, the electro-optic effect can introduce a fast response for switching states but it is not compatible to silicon photonic platform due to the small electro-optic coefficient of silicon material. In contrast, the phase shift which is based on the thermo-optic effect can be attained by heating the waveguide with a metallic microheater. This mechanism could be fabricated using the uncomplicated CMOS processes, which still respond to the short switching time in several microseconds. Furthermore, this mechanism can permit ignorable optical losses by locating the lossy microheater at a reliable distance from the waveguide. Nevertheless, such a heater is usually placed far from the core waveguide, which could lead to low-performance on aspects of high power consumption or low switching speeds. Thermo-optic phase shifters are applied in a wide range of current and new integrated photonic applications such as phased arrays [15–17] beam steering [18], reconfigurable photonics [19–21] integrated quantum photonics [22], [23] and neural networks [24], [25]. Especially, thermo-optic phase shifters are indispensable elements in silicon photonic devices since optical phase manipulations are essential to divide or recombine optical patterns. However, for TO devices based on metallic microheaters [26–29] the influence of the upper-cladding material showing a trade-off between the power consumption and the switching speed [30]. Hence, an acceptable way to improve electrical performance is to reduce the gap between the core waveguide and the microheater. Several two dimensional materials, for example, graphene as a transparent heater, have been chosen to reduce the gap [31], [32]. However, graphene has a relation to complex fabrication processes that have not been yet prepared for massive manufacture. In such a scenario, transparent conducting oxides (TCOs) have been considerably interested in active photonic devices due to their high transparency, good conductivity, and excellent adhesion to substrates. Among the existing TCOs, Indium Tin Oxide (ITO) is being expected as a promising potential to achieve a plethora of efficient electro-optic active devices [33–36]. Because, when electrically tuned, ITO films can deliver unity-strong index modulation [18], [37], incredibly close to its epsilon-near-zero (ENZ) regime in the near-infrared spectrum [38], [39], which leads to inter alia to significant optical nonlinearities [40], [41], and slow-light effects [42]. In the field of silicon photonics, this uniquely specific feature has been utilized to construct high-performance devices since optical losses are significantly reduced in the ENZ regime. One of the significant interests surrounding ITO is to realize its applied potential as controllable and ultra-low loss phase shifters for wide silicon photonic active devices [43], [44].

In MDM systems, multimode converter (MMC) [45], and multimode selective router (MSR) [10] are vital elements for realizing a flexible mode processing system. In this paper, we propose and design transparent ITO heaters for high-performance TO tuning of silicon photonic structures based on numerical simulation processes. The ultra-low loss ITO heater is utilized to realize compact and high bandwidth mode selective devices with significant performances of low-loss, ultra-low crosstalk, large fabrication tolerance, low power consumption, and short switching time. The spacing influence between the core waveguide and the ITO microheater and the geometrical optimizations of silicon photonic devices based on ITO phase shifters are investigated and characterized for TE polarization.

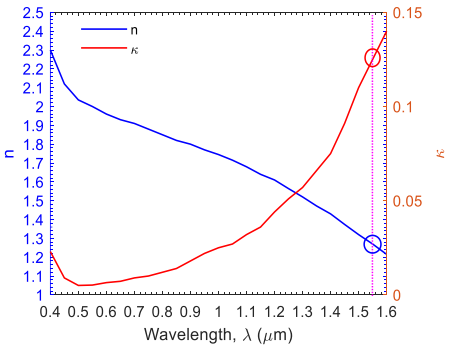

Fig.1. *Spectral behavior of real (blue) and imaginary (red) parts of the refractive index of ITO obtained from sputtered films by using different oxygen flow-rate and the post-deposition heat treatment process.*

II. MATERIALS AND METHODS

Current photonic integrated circuits mainly utilize phase modulation to control the light signals. One of the most popular phase modulation methods is to change the refractive index, *n*, and Kramers-Kronig (K-K) relations through electro-optic, thermo-optic, or carrier effects. Optical performances of a photonic integrated device strongly depend on lower physical mechanisms, especially to carrier effect relating to optical loss due to conductive absorption caused by doped particle population. ITO material can be used as an electro-optic (EO) case in the *n*–dominant regime or for the electro-absorptive (EA) cases in the *κ*–dominant regime depending on the biased carrier condition and relative position to the epsilon-near-zero (ENZ) point. The optical property of ITO ($e = e' + je''$) in the telecom window of the near infrared spectrum can be described by the Lorentz-Drude model [44]:

$$\varepsilon = \varepsilon_{\infty}\left(1 - \frac{\omega_p^2}{\omega^2 + j\omega\Gamma}\right) \tag{1}$$

where w is the angular frequency, e_{∞} is high-frequency permittivity, Γ is the damping factor and w_p is so-called as the plasma frequency that is defined by:

$$\omega_p = \sqrt{\frac{Ne^2}{\varepsilon_0 \varepsilon_{\infty} m^*}} \tag{2}$$

where e=1.6×10^{-19} C is the elementary charge of electron, e_0 = 8.8541878128×10^{-12} F·m^{-1} is the vacuum permittivity, m^* is the electron effective mass, and N is the

bulk free carrier concentration. Drude parameters are determined as: e_∞ = 3.9, Γ = 1.8×10^{14} rad/s and m^* = $0.35m_e$, m_e is the free electron mass [44].

The resistivity r caused by ITO-based thin film can be attained as follows [44]:

$$\rho = \frac{\Gamma m^*}{Ne^2} \quad (3)$$

At a low-doped concentration ($N = 10^{19}$ cm^{-3}) ITO supplies both characteristics of high-transparency ($e'' \approx 0$) and high-resistivity. When the concentration is lower this level, ITO acts as a Mott insulator and becomes no longer conducting [38]. Otherwise, the light-matter interaction is considerably enhanced closely to the ENZ regime ($N = 6.5 \times 10^{20}$ cm^{-3}), where $e' = 0$, $e'' > 0$ and $|\varepsilon|$ achieves its minimum value ($|\varepsilon| = 0.57$). As a result, optical losses may be drastically increased and thus, the transparency condition may be lost. However, when the lower-doped ITO, the resistivity becomes quite high leading the response time for switching larger. This can limit the promising potential for ultrafast applications. Therefore, in this paper, a free carrier concentration level of N=3 × 10^{20} cm^{-3} is chosen. Fig. 1 exhibits the refractive index parameters of (n,k) of ITO as a function of the wavelength when the free carrier concentration of N is 3 × 10^{20} cm^{-3}. At this value of the free carrier concentration, substituting into Exp. (1) we obtain $n + jk$ =1.27+j0.125. This value is also suitable to the experimental measurement results obtained from the sputtered films using the oxygen flow-rate and the post-deposition heat treatment process [37].

In this investigation, multiphysics and FEM numerical simulation tools of the Rsoft commercial simulation software are manipulated to characterize performance of ITO phase shifters with mesh sizes of $\Delta x = \Delta y = \Delta z$ =5 nm. The designated ITO phase shifters are applied for designing multimode selective devices. The proposed devices based on silicon photonic waveguides are implemented and optimized using the three-dimensional beam propagation method with ideal grid sizes.

III. STRUCTURE DESIGN AND SELECTION OF THE ITO PHASE SHIFTER

The structural model of a ITO phase shifter is shown in Fig. 2(a), including a ITO thin film placed on the top of a silicon core waveguide. It is well-known that thermo-optic phase shifters are widely implemented in silicon photonics because of CMOS technology compatibility and the thermo-optic coefficient is sizeable with the bulk silicon crystal. When propagating the light field through the thermal phase shifter, under the impact of the heat flow that caused from the ITO heater in metallic state by a voltage source, the refractive index of waveguide Si can be tuned by changing the temperature of the phase shifter. This process leads a phase shift that can be determined by following relation [46]:

$$\Delta\Phi = \frac{2\pi L_{PS}}{\lambda_0}\frac{dn}{dT}\Delta T \quad (4)$$

where L_{PS} is the ITO heater length in the propagation direction, λ_0 is the operation wavelength, $\Delta T = T - T_0$ is the temperature change in the silicon waveguide core (T_0 = 300K is the room temperature), $\frac{dn}{dT}$ is the thermo-optic coefficient for silicon material, and $\frac{dn}{dT} = 1.84\times10^{-4}\,K^{-1}$ at the 1550-nm wavelength and at room temperature.

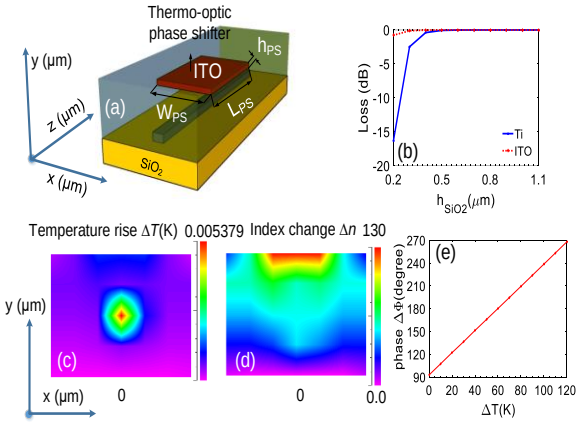

Fig. 2. Thermo-optic phase shifter based on ITO: (a) the structural diagram of a ITO phase shifter, (b) the simulated loss of Ti and ITO-based phase shifters depending on the silica gap between the silicon core layer and the microheater, (c) the temperature rise distribution on the ITO phase shifter simulated by using the multiphysics tool, (d) the index change distribution on the ITO phase shifter simulated by the multiphysics tool, and (e) the phase shift depending on the temperature change.

It is noted that the performance of the phase shifter does not depend on the heater length because the ITO heater length, L_{PS}, can be neglected since we combine both heat and optical phase shift equations. Hence, the same phase shift is induced for a given power consumption without considering the heater length [29]. In a thermo-optic phase shifter, the thermal conductivity reduction can improve the electric power consumption level by order of magnitude, but the switching time is usually worse to the same degree. Also, reducing the heater cross-section may lead to a rise in the current density and could melt the heater. Furthermore, the driving voltage will also be higher, and a more stringent alignment must be required if the heater is narrowed to the same order of the core waveguide width. Considering the thickness, fabricating the homogeneous and high-quality ITO thin-film structure becomes harder for thicknesses lower than 100 nm. As a result, in this study, three geometrical parameters, including the width W_{PS}, the length L_{PS}, and the thickness h_{PS} of the ITO heater, are set as 1 μm, 200 μm, and 100 nm, respectively.

Many TO phase shifters utilizing various materials such as Ti, ITO, Ag have been investigated in scientific reports. For a given metallic heater, the plasmonic effect can hybridize photonic mode propagating into silicon waveguide due to resonant condition at the metal-dielectric

interface if the gap between metallic and silicon layers is small enough in several nanometer scales. This effect absorbs the photonic mode, thus limiting the propagation length of the optical field in the total inner reflection mechanism. To avoid the influence of the plasmonic effect, the gap of the silica layer sandwiched between the ITO and silicon layers is typically chosen as h_{SiO_2} = 1 μm [47]. Fig. 2(b) shows the propagation loss of the light when passing through the thermo-optic phase shifters, made from Ti and ITO, depending on the gap h_{SiO_2} by using the multiphysics simulation tool. Simulated results show that the phase shifter made from Ti heater is more strongly influenced by the plasmonic effect than that of the ITO heater. When the gap is higher than 0.6 μm, the conductive losses due to the plasmonic effect are negligible for both Ti and ITO heaters. The distributions of the temperature rise (ΔT) and the index change (Δn) in the core layer are correspondingly shown to Fig. 2(c) and Fig. 2(d) by using the multiphysics tool when the ITO phase shifter is supplied by the electric power to achieve the tuned phase of π radian. In this work, the phase difference is changed from – π/2 to π/2 by the temperature rise (ΔT). As seen in Fig 2(e), the temperature rise changes from 0K to 120K to achieve the phase difference from 90 degrees to 270 degrees.

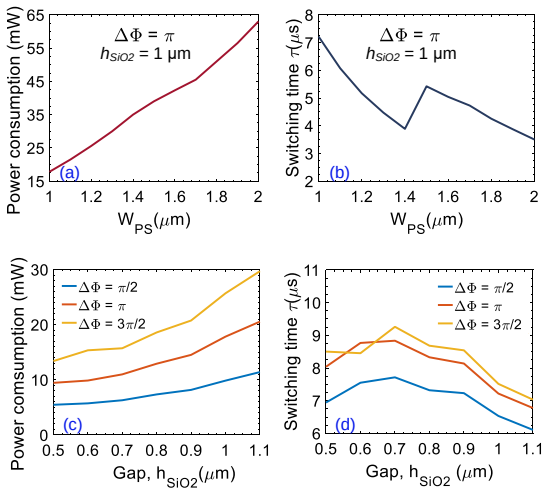

Fig. 3. *ITO phase shifter characterizations: (a, b) the electric power consumption and the switching time as functions of the ITO microheater width when fixing the silica gap to reach the phase shift of π (radians), and (c,d) the electric power consumption and the switching time within the dependence on the silica gap at the ITO heater width of 1 μm for different shifted phase angles (π/2, π,*

The power consumption of the phase shifter is estimated by the needed power to tune the desired phase of π radians (P_π). To evaluate the efficient function of a thermo-optical switch, we should consider the electric power consumption. For a given thermo-optic phase shifter, we require to obtain the optimal product of $P_\pi.\tau = H.\Delta T_\pi$ during the switching operation process. Here, H stands for the heat capacity, ΔT_π is the changing temperature from a cold state to a hot state to attain the expected phase shift of π, and τ is the switching time relating to the phase shifter temporal response and the cut-off frequency $f_{cut\text{-}off}$ [48]. The switching power consumption is estimated by using a modified two-dimensional treatment of heat flow on the lateral spreading.

The switching electric consumption power is determined by the following equation utilizing a modified two-dimensional treatment of the heat flow on the lateral spreading [49]:

$$P_\pi = \frac{\lambda \kappa_{SiO_2} \left(\frac{W_{PS}}{h_{SiO_2}} + 0.88 \right)}{\left| \frac{dn}{dT} \right|_{Si}} \quad (5)$$

where κ_{SiO_2} =1.4 W/(m.K) is the thermal conductivity of SiO_2, λ is the operation wavelength, and W_{PS} is the width of the ITO heater on the lateral direction.

The switching time can be considered as a consequence of the required response time of the heat flow propagation from the micro-heater to the silicon core layer along the active length of the ITO phase shifter, which relates to the consumption power by the formula [26], [48]:

$$\tau = \frac{\pi \lambda \rho_{SiO_2} C_{SiO_2} A}{e P_\pi \left| \frac{dn}{dT} \right|_{Si}} \quad (6)$$

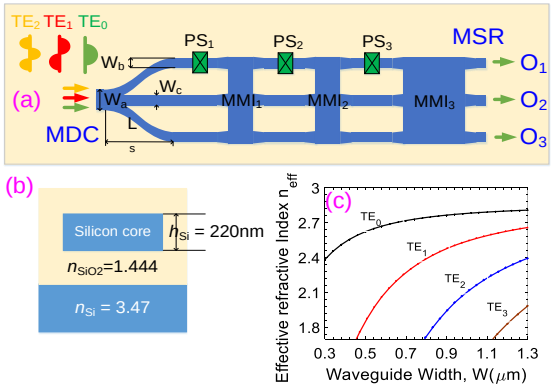

Fig. 4. *A design of the multimode selective router (MSR) using ITO phase shifters based on silicon photonic waveguides: (a) top-view structural diagrams of a three-mode converter and a three-mode selective router, (b) the side-view of designated silicon photonic structures, and (c) the mode profile characterized by the effective refractive index on according to the input waveguide width solved by the mode solver tool of the Rsoft commercial software.*

where ρ_{SiO_2} =2.203 g/cm^3 is density of silica, C_{SiO_2} =0.703 J/(g.K) is specific heat capacity of silica, $A = (2L_{th} + W_{PS})(h_{Si} + h_{SiO_2})$ is the effectively heated cross-section area relating to geometry parameters of the ITO phase shifter, h_{Si} = 220 nm is the thickness of the silicon core, $e \approx 2.7182818$ is the natural logarithm constant. L_{th} is the thermal diffusion length measured by taking the distance where the maximum temperature laterally decreased at $1/e^2$ away from the silicon waveguide.

The electric power consumption and the switching time are crucial parameters depending on geometrical structures such as the gap h_{SiO_2} and the ITO heater, plotted in Fig. 3. Figs. 3(a,b) show the power consumption (P_π) and the switching time (τ) of the designated ITO phase shifter as functions of the width W_{PS} when the silica gap h_{SiO_2} is kept as 1 μm. The electric power consumed to reach the needed phase increases when the gap h_{SiO_2} increases. Therefore, in order to minimize the consumed power, the width W_{PS} is chosen as 1 μm which still attains the short switching time about 7 μs for the shifted phase of π radians. Noted that, in Fig. 3(b), when the width W_{PS} is in the range from 1.4 μm to 1.5 μm, the switching time τ increases because the effective cross-section area strongly increases. Also, when the width W_{PS} is fixed by 1 μm, the dependence of the power consumption (P_Φ) and the switching time (τ_Φ) on the gap h_{SiO_2} for several values of the phase shift Φ (π/2, π, 3π/2) are exhibited corresponding to Fig. 3(c,d), respectively. As a rule, the power consumption is an increasing function versus the gap. However, after reaching the highest point at the gap of h_{SiO_2} = 0.7 μm, the switching time decreases when the gap increases further. To achieve the phase difference of π/2, π, 3π/2, the electric power consumptions are corresponding to 9.85 mW, 17.83 mW, and 25.69 mW, and the time responses are corresponding to 6.53 μs, 7.2 μs, and 7.51 μs at the selected gap of h_{SiO_2} = 1 μm, respectively. All power consumption and switching time levels for the TO tuning phase are about some tens of milli-Watts and several microseconds, respectively, which are acceptable in the integrated photonic devices.

IV. APPLICATIONS OF THE ITO PHASE SHIFTER IN OPTICAL MODE SELECTIVE ROUTER

For a given MDM system, a multimode selective router exploiting the mode routing function plays an indispensable role for a flexible mode division processing system. In this study, the schematic design of a three-mode selective router is sketched as seen in Fig. 4(a). This structure is constructed from fundamental elements composing of 3×3 multimode interference (MMI) couplers, symmetric Ψ-junction couplers, and ITO thermo-optic phase shifters. The proposed device is designed and simulated by using channel structural waveguides based on the SOI material platform with the 220nm-silicon thickness, and a cladding layer covered by the silica layer (SiO_2) (Fig. 4(b)). On the top structure, an ITO thin-film layer, whose structural parameters have been initially installed as mentioned above, is applied as TO phase shifters for realizing the mode selective functions. The device is designed in the transverse electric (TE) polarization regime and for the third telecom window with the central operation wavelength λ=1550 nm. The proposed device can be patterned from Deep Ultraviolet (DUV) photolithography with an illumination wavelength of 193-nm [50] and inductively coupled plasma (ICP) etching processes [51]. The ITO thin film can be easily formed with excellent quality via various deposition methods such as atomic layer deposition [52], pulsed layer deposition [53].

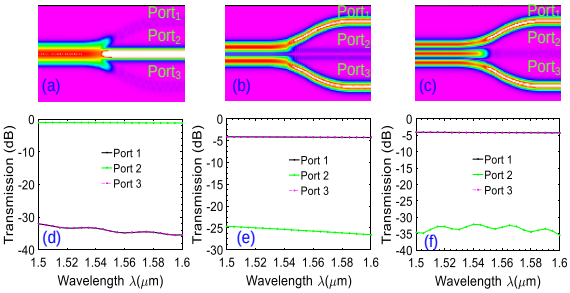

Fig. 5. *The operating principle of the mode decomposer based on a symmetric Ψ-junction: (a, b, c) electric field patterns of the mode propagation corresponding to TE_0, TE_1, and TE_2 mode, respectively, (d-f) transmission spectral responses at output ports following the input modes of TE_0, TE_1, and TE_2 mode, respectively.*

4.1. Symmetric Ψ-junction

A symmetric Ψ-junction, which acts as a mode decomposer (MDC), is specially designed to convert higher order-modes into fundamental mode. Following the mode-sorting principle suggested by Riesen and Love et al. [54], if the effective index of the input is matched with the effective index of the fundamental mode in the output, the fundamental mode exists in these outputs. It is well-known that the effective index of the fundamental mode is the highest compared to all modes. Therefore, the larger waveguide has a higher effective index than the smaller waveguides. In this design, the outer waveguide width (W_b) of the MDC structure is narrower than the inner output waveguide width (W_c). Hence, the fundamental mode TE_0 will connect to the inner waveguide, and two higher-mode are converted to two TE_0 mode components at two outer arms with equal amplitudes. However, two phases of two outer arms are out of phase when the input mode is TE_1. In contrast, two phases of two outputs are in phase when the input mode is TE_2. We apply the numerical simulation technique based on the three-dimensional semivectorial beam propagation method (3D SV-BPM) to solve effective indexes of three lowest-order TE modes, plotted in Fig. 4(c). As a rule, we choose the input width of the MDC structure equally to W_a = 1.3 μm to support three guided modes, including TE_0, TE_1, TE_2. Two sinusoidal bending waveguides have the length L_s= 120 μm and the width W_b = 0.5 μm. A straight waveguide in the middle is chosen W_c = 0.6 μm that only supports TE_0 mode. Fig. 5(a, b, c) show the results of decomposed mode components for both TE_0, TE_1, and TE_2 input modes when coupling to the MDC input. In MDC, the fundamental mode is propagated to the straight waveguide in the middle output waveguide of the Ψ-junction junction. Meanwhile, the first and the second-order mode is coupled to the outer arms at the output. Fig. 5 (d, e, f) illustrate wavelength responses of transmission curves corresponding to injected modes of TE_0, TE_1, TE_2, respectively. The simulated results show that, in all cases,

transmission losses are smaller than 0,5 dB in broadband of 100-nm wavelength, and crosstalk is always lower than -25 dB for the undesired output ports.

4.2. 3×3 multimode interference couplers

Three kinds of 3×3 MMI couplers are used in these designs (so-called as MMI_1, MMI_2, and MMI_3 couplers). The width of multimode interferences is designed ideally to W_{MMI} = 6.8 μm. The length of MMI_1, MMI_2, and MMI_3 couplers correspond to L_{MMI_1}, L_{MMI_2}, L_{MMI_3}, respectively. Three input ports of three kinds of mentioned MMI couplers are placed at specific positions of $-W_{MMI}/3$, 0, $W_{MMI}/3$ along the *x*-coordinate, respectively. Noted that the symmetrical line goes through the central line of multimode structures. MMI_1 and MMI_2 couplers are ideal structures, which are 3×3 MMI couplers with their lengths $L_{MMI_1} = L_{MMI_2} = 3L_\pi/8$. While MMI_3 is a 3×3 MMI coupler that its length is defined as $L_{MMI_3} = 3L_\pi/2$ for exploiting the function of a 3 dB-coupler. Herein, L_p is a specific length of MMI coupler, so-called as the half-beat length, which is determined by the following equation [55]:

$$L_\pi = \frac{4n_e W_e^2}{3\lambda} \tag{7}$$

where $W_e = W_{MMI} + \frac{\pi}{\lambda}\left(n_e^2 - n_c^2\right)^{-1/2}$ (for TE polarization mode)

Tab. 1. Geometrical parameters of the proposed multimode selective devices.

Parameter	Value	Parameter	Value
L_{MMI_1}	44 μm	H_{PS}	100 nm
L_{MMI_2}	44 μm	W_{PS}	1 μm
L_{MMI_3}	176 μm	L_{PS}	120 μm
W_{MMI_1}	6.8 μm	W_a	1.3 μm
W_{MMI_2}	6.8 μm	W_b	0.5 μm
W_{MMI_3}	6.8 μm	W_c	0.6 μm
L_{PS}	200 μm	h_{SiO_2}	1 μm

In which, n_e is the effective refractive index, n_c is the refractive index of the cladding layer, and λ is the operation wavelength of the device. Following the general interference (GI) principle, the self-imaging is periodically reproduced along the propagation direction of the z-coordinate. Fig. 6(a, b) present the simulated electric field patterns for MMI_1 and MMI_2 couplers, and Fig. 6(c, d) exhibit the simulated fields for the MMI_3 coupler when

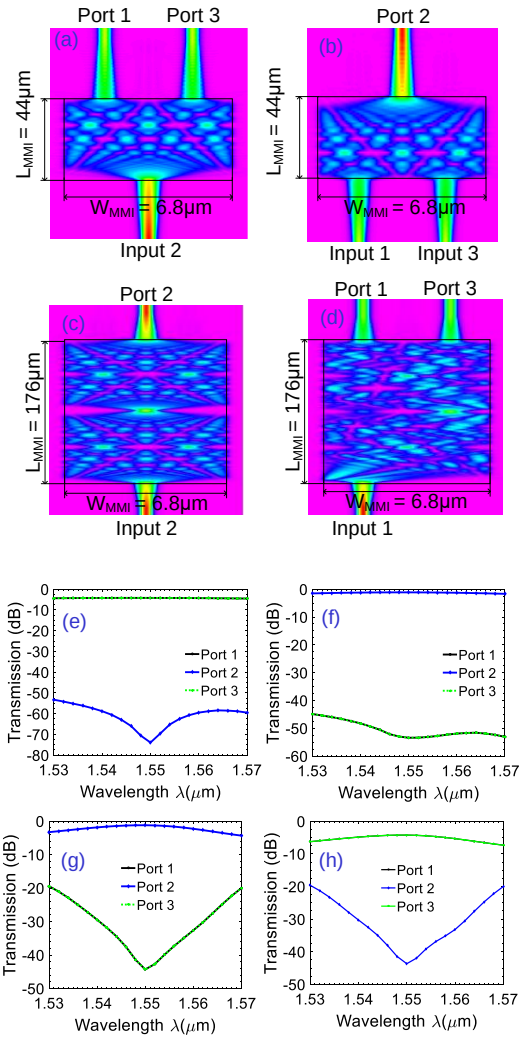

Fig. 6. *Simulated operations of different 3×3 multimode interference couplers: (a) optical power splitting operation for MMI_1 and MMI_2 couplers when injecting the optical field at the central port, (b) optical power combining operation for MMI1 and MMI2 couplers at the central ports when injecting two in-phase optical fields at two outer arms, (c) the self-imaging process when injecting the optical field at the central input waveguide of the MMI_3 coupler,(d) the operating principle as a 3-dB coupler for two outer arms of the MMI_3 coupler, and (e-h) simulated spectral behaviors of different 3×3 MMI couplers corresponding to cases of (a-d), respectively.*

their lengths are optimized to attain the highest transmissions. For MMI_1 and MMI_2 couplers, the input light is injected to input 2 of the MMI1 coupler, the crosstalk is lower than -50 dB, and fluctuation of propagation loss is lower than 0.3 dB in the 40-nm wavelength response. When two input lights are coupled to input 1 and input 3 of MMI_1 and MMI_2 couplers, the power transmission at each desired output port is smaller than -1 dB, and the crosstalk at port 1 and port 3 are less than -45 dB in the wide band of 40-nm, as seen in Fig. 6(e, f). Also, for the MMI_3 coupler, one can see that a low transmission loss level of -1 dB is numerically measured with -44 dB of crosstalk at the wavelength of 1550 nm when the light field is injected into its central input port, as shown in Fig. 6(g). Also, the optical transmission spectrum of the MMI_3

coupler when guiding the light fields into its input 1, which plays the role of the 3-dB coupler, is illustrated in Fig. 6(h). It is seen that the desired powers at 1550 nm are about -4 dB while crosstalk is about -44 dB. In this work, all parameters optimized by simulation are listed in Tab. 1.

The transfer matrices of MMI_1 and MMI_2 couplers when injecting optical fields placed at specific positions above are deduced via relatively simple algebra formulation processes from the interference theory, that was suggested from Soldano et al. [55] by:

$$M = \begin{pmatrix} \frac{1}{2}e^{j\frac{p}{2}} & \frac{1}{\sqrt{2}} & \frac{1}{2}e^{j\frac{2p}{3}} \\ \frac{1}{\sqrt{2}} & 0 & \frac{1}{\sqrt{2}} \\ \frac{1}{2}e^{j\frac{2p}{3}} & \frac{1}{\sqrt{2}} & \frac{1}{2}e^{j\frac{p}{2}} \end{pmatrix} \quad (8)$$

Also, the transfer matrix of the MMI_3 coupler when access waveguides are placed at specific positions above is:

$$N = \begin{pmatrix} \frac{1}{\sqrt{2}} & 0 & \frac{1}{2}e^{j\frac{p}{2}} \\ 0 & 1 & 0 \\ \frac{1}{2}e^{j\frac{p}{2}} & 0 & \frac{1}{\sqrt{2}} \end{pmatrix} \quad (9)$$

where φ, is the accumulative phase angle when passing through the MMI_1 and MMI_2 couplers, θ is the accumulative phase angle when travelling the MMI_3 coupler.

4.3. Operating principle and structural optimization of three-mode selective router

This section proposes a novel design of a three-mode selective router (TSR) based on three MMI couplers, an MDC, and three ITO thermo-optic phase shifters, expressed in Fig. 4(b). The Ψ-junction-based MDC is placed at the MSR input port for decomposing the guided modes to fundamental modes. Two ideal 3×3 MMI couplers, namely MMI_1, MMI_2 with the length of $3L_\pi/8$, are concatenated later. At the last stage, a 3×3 MMI coupler, namely MMI_3 with a length of $3L_\pi/2$, is responsible for the mode routing mission.

Next, we analyze the working mechanism of three guided modes into the proposed router. First, in the case of input mode is TE_0. This mode is coupled to the central output port of the Ψ-junction coupler. It then is guided into the input port of the MMI1 coupler and is divided into two of its outer output arms with in-amplitude and in-phase according to the transfer matrix from Exp. (8) and Exp. (9). These optical paths are led to the MMI_2 coupler via the phase shifter of PS_2. If the phase difference $\Delta\Phi_2$=0, two optical signals will be straightforwardly directed to two outer arms of the MMI3 that one arm is traveled the phase shifter PS_3. The MMI_3 plays the role of a 3-dB coupler for two outer optical paths because the MMI3 coupler length is $3/2L_\pi$. Hence, if the phase shifter $\Delta\Phi_3$ is $\pi/2$, the MMI_3 coupler will combine two optical signals at the output port

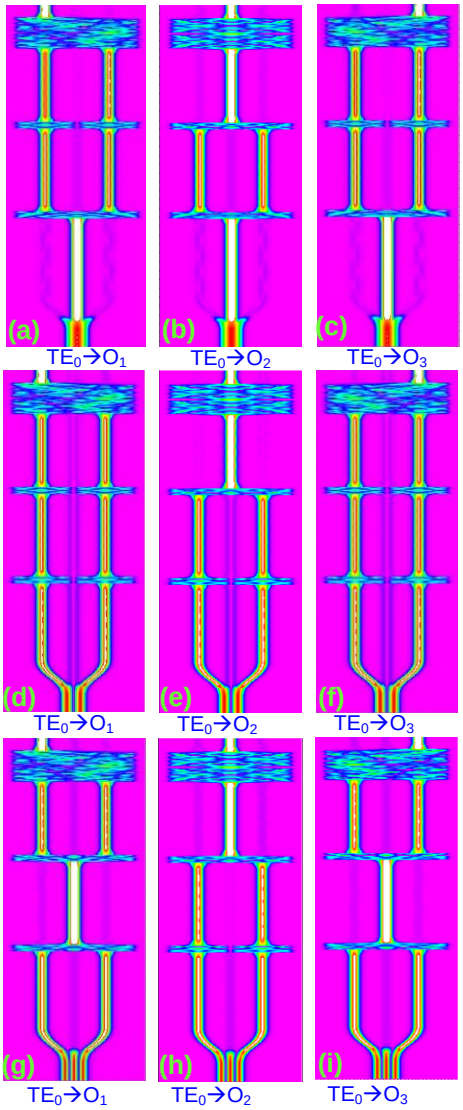

Fig. 7. *Stimulated electric field patterns of the three-mode selective router: (a-c) for the inputs of TE_0 modes, (d-f) for the inputs of TE_1 modes, and (g-i) for the inputs of TE_2 modes.*

O_1. If the phase shifter $\Delta\Phi_3$ is $-\pi/2$, MMI_3 will combine two optical signals at the output port O_3. In another scenario, if the phase shift $\Delta\Phi_2$ is π, the combined optical signals will be focused on a unique signal at the central input port of the MMI_3 coupler. That reason is due to the MMI_3 length as $3L_\pi/2=2\times3L_\pi/4$, thus following the symmetric interference rule, this optical field is reproduced at the central output port O_2 of the MMI_3 coupler.

Assume that the input mode at the stem of the Ψ-junction coupler is the TE_1 mode. It is decomposed into a pair of fundamental modes at two outward branches of the Ψ-junction coupler with the same magnitude and out of phase. If phase shift $\Delta\Phi_1$ is 0, these two signals will continue to be straightforwardly transmitted through the output arms of MMI_1. Depending on the phase shift status of the PS_2, optical signals are routed to different outputs. If $\Delta\Phi_2 = 0$, these two routes continue to pass through the MMI_2 coupler before reaching the MMI_3 coupler. At the last stage, if $\Delta\Phi_2 = \pi/2$, the optical signal is combined at the output O_1, and vice versa, if $\Delta\Phi_2 = -\pi/2$, the optical signal

is switched to the output O_3. In order for TE1 mode to be switched to the output O_2, the phase shift action of PS_2 needs to be controlled so that $\Delta\Phi_2 = \pi$, then the two optical lines will be combined at the central output port of MMI_2 and directed to the output O_2 because of the symmetrical interference property of the MMI_3 coupler.

Analogously, we also get the non-blocking activities of TE_2 mode. It means TE_2 mode can be optionally switched to the three outputs of the proposed router freely. We note that the non-invasive action between TE_1 and TE_2 modes is because mode TE_2 will be coupled with two output arms with the same amplitude but out of phase. Nine simulated electric field distributions for independent mode selective states of the designated router when injecting three guided modes of TE_0, TE_1, and TE_2 are exhibited correspondingly to Fig. 7 (a-i), respectively. It is visible to see that all cases are exact to the theoretical analysis.

4.4. Characterization of the proposed mode converter and mode selective router and discussion

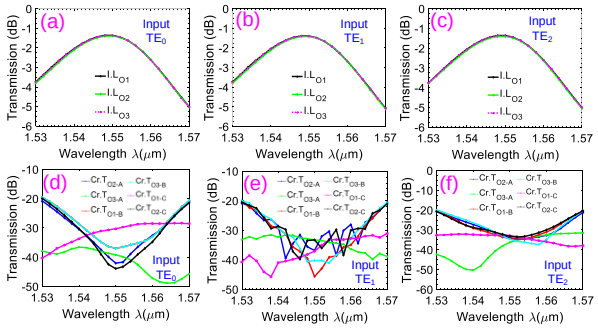

Fig. 8*. Numerically stimulated wavelength spectrum responses of the MSR: (a, b, c) are insertion loss transmissions at output ports of the TSR structure, and d, e, f) are crosstalk transmissions at output ports of the TSR structure, according to input signals of TE_0, TE_1, TE_2, respectively.*

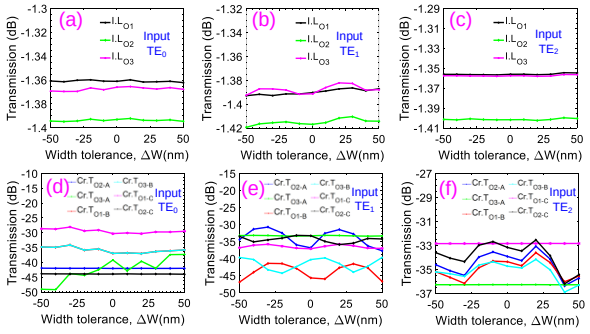

Fig. 9. *Numerically stimulated width tolerances of the TSR: (a, b, c) are insertion loss transmissions at output ports of the TSR structure, and (d, e, f) are crosstalk transmissions at output ports of the TSR structure, according to input signals of TE_0, TE_1, TE_2, respectively.*

Optical losses when traveling through the designed ITO phase shifter were negligible in agreement with the simulation result. Likewise, the sidewall roughness losses could be trivial if a high-resolution photolithography process is applied to fabricate proposed devices. Therefore, in optical characterizations, insertion loss (I.L) caused by propagation and radiation losses and crosstalk (Cr.T) caused by undesirable optical sources are considered critical contributions for device's optical performances. Fig. 8(a-f) show the simulated spectrum of the TMC structure in a broadband of 100-nm wavelength for the 3-dB bandwidth with the suggested ITO phase shifters corresponding to input signals of TE_0, TE_1, TE_2, respectively. As a result, 3-dB wavelength bandwidths of the I.L transmission in nine cases, which are measured from simulated data, show a high wavelength spectrum of 40-nm from 1530-1570 nm while assuring crosstalk always lower than -20 dB. Herein, we denote A, B, and C cases corresponding to the optical modes switched to the desired output ports of O_1, O_2, and O_3, respectively. Furthermore, in this work, the designated devices can be arranged in a compact footprint of 8 μm×2160 μm.

In integrated silicon photonics, the devices always suffer some errors from the manufacturing process that are caused from the resolution limit of the fabrication technology and the purity of supplied SOI wafer. Hence, the fabrication tolerances are necessary for photonic integrated circuits, especially for simulation-based designs. The I.L variation is also tiny for three guided modes in the TSR device, about 0.02 dB in ±50 nm width tolerance while keeping the Cr.T level lower than -28 dB for three guided modes, as seen in Fig. 9(a-f). Fig. 10(a-f) depict the I.L and Cr.T transmissions depending on the length tolerance Δh of the silicon thickness for the TSR structure. It can be seen that

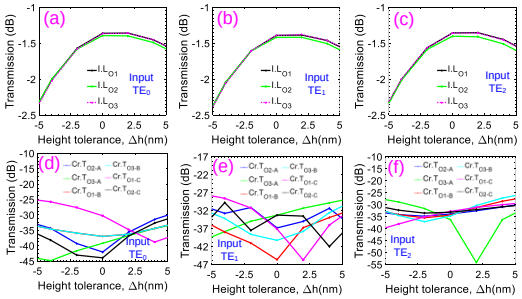

Fig. 10. *Numerically stimulated height tolerances of the TSR: (a, b, c) are insertion loss transmissions at output ports, and (d, e, f) are crosstalk transmissions at output ports of the TSR structure, according to input signals of TE_0, TE_1, TE_2, respectively.*

I.L fluctuates slightly from -1.1 dB to -1.81 dB for TMC in a relatively large tolerance of Δh=±5 nm. Also, I.L fluctuates in a small gap from -1.4 dB to -2.3 dB, and Cr.T is not higher than -25 dB in a height tolerance of Δh=±5 nm. The current advanced fabrication technology, such as 193-nm photolithography, can obtain such tolerances.

5. Conclusions

In summary, we presented a design of compact and high bandwidth mode selective router based on silicon-on-insulator waveguides, which can achieve multiple functions of a three-mode selective router by tuning the phase shift via low-loss ITO thermo-optic phase shifters. Simulation results have demonstrated the 3-dB bandwidth for the three-mode converter and three-mode selective router as much as 100-nm and 40-nm while preserving crosstalk under -25 dB, respectively. Besides, the

designated device also had relatively large fabrication tolerances corresponding to width and height tolerances of ±50 nm and ±5 nm, respectively. The proposed device consumed a low power consumption not exceeded 90 mW and spent a short time below 8 μs in switching the operating states. Moreover, the proposed photonic router can be integrated into a compact footprint of 8 μm×2160 μm. Such excellent performances of the proposed structures make designed devices a promising potential for applications in high-speed mode division multiplexing systems and very large-scale photonic integrated circuits.

REFERENCES

1. T. Morioka, Y. Awaji, R. Ryf, P. Winzer, D. Richardson, and F. Poletti, "Enhancing optical communications with brand new fibers," *IEEE Commun. Mag.* **50**, 31–42 (2012).
2. E. Granot and S. Sternklar, "Limitations to bit-rate and spatial capacity of an optical data transmission channel," J. Opt. A **4**, 2–4 (2002).
3. A. D. Ellis, J. Zhao, and D. Cotter, "Approaching the Non-Linear Shannon Limit," J. Light. Technol. **28**, 423–433 (2010).
4. K. Roberts, Q. Zhuge, I. Monga, S. Gareau, and C. Laperle, "Beyond 100 Gb/s: Capacity, flexibility, and network optimization [invited]," *J. Opt. Commun. Netw.* **9**, C12–C24 (2017).
5. X. Wang, F. Zhou, S. Yan, Y. Yu, J. Dong, and X. Zhang, "Broadband on-chip integrator based on silicon photonic phase-shifted Bragg grating," *Photonics Res.* **5**, 182 (2017).
6. A. M. Bratkovsky, J. B. Khurgin, E. Ponizovskaya, W. V. Sorin, and M. R. T. Tan, "Mode division multiplexed (MDM) waveguide link scheme with cascaded Y-junctions," *Opt. Commun.* **309**, 85–89 (2013).
7. D. Guo and T. Chu, "Silicon mode (de)multiplexers with parameters optimized using shortcuts to adiabaticity," *Opt. Express* **25**, 9160 (2017).
8. D. Dai and M. Mao, "Mode converter based on an inverse taper for multimode silicon nanophotonic integrated circuits," *Opt. Express* **23**, 28376 (2015).
9. B. Stern, X. Zhu, C. P. Chen, L. D. Tzuang, J. Cardenas, K. Bergman, and M. Lipson, "On-chip mode-division multiplexing switch," *Optica* **2**, 530 (2015).
10. R. B. Priti, H. P. Bazargani, Y. Xiong, and O. Liboiron-Ladouceur, "Mode selecting switch using multimode interference for on-chip optical interconnects," *Opt. Lett.* **42**, 4131–4134 (2017).
11. X. Wang and K. S. Chiang, "Polarization-insensitive mode-independent thermo-optic switch based on symmetric waveguide directional coupler," *Opt. Express* **27**, 35385 (2019).
12. A. Masood, M. Pantouvaki, D. Goossens, G. Lepage, P. Verheyen, J. Van Campenhout, P. Absil, D. Van Thourhout, and W. Bogaerts, "Fabrication and characterization of CMOS-compatible integrated tungsten heaters for thermo-optic tuning in silicon photonics devices," *Opt. Mater. Express* **4**, 1383 (2014).
13. M. Takenaka, Y. Kim, J. Han, J. Kang, Y. Ikku, Y. Cheng, J. Park, M. Yoshida, S. Takashima, and S. Takagi, "Heterogeneous CMOS Photonics Based on SiGe/Ge and III-V Semiconductors Integrated on Si Platform," *IEEE J. Sel. Top. Quantum Electron.* **23**, (2017).
14. D. Inoue, T. Ichikawa, A. Kawasaki, and T. Yamashita, "Silicon optical modulator using a low-loss phase shifter based on a multimode interference waveguide," *Micromachines* **10**, (2019).
15. S. A. Miller, Y.-C. Chang, C. T. Phare, M. C. Shin, M. Zadka, S. P. Roberts, B. Stern, X. Ji, A. Mohanty, O. A. Jimenez Gordillo, U. D. Dave, and M. Lipson, "Large-scale optical phased array using a low-power multi-pass silicon photonic platform," *Optica* **7**, 3 (2020).
16. J. Sun, E. Timurdogan, A. Yaacobi, E. S. Hosseini, and M. R. Watts, "Large-scale nanophotonic phased array," *Nature* **493**, 195–199 (2013).
17. J. Sun, E. Timurdogan, A. Yaacobi, Z. Su, E. S. Hosseini, D. B. Cole, and M. R. Watts, "Large-scale silicon photonic circuits for optical phased arrays," *IEEE J. Sel. Top. Quantum Electron.* **20**, (2014).
18. R. Amin, R. Maiti, J. K. George, X. Ma, Z. Ma, H. Dalir, M. Miscuglio, and V. J. Sorger, "A Lateral MOS-Capacitor-Enabled ITO Mach-Zehnder Modulator for Beam Steering," *J. Light. Technol.* **38**, 282–290 (2020).
19. D. Dai, "Silicon Nanophotonic Integrated Devices for On-Chip Multiplexing and Switching," *J. Light. Technol.* **35**, 572–587 (2017).
20. F. Testa, S. Tondini, F. Gambini, P. Velha, A. Bianchi, C. Kopp, M. Hofbauer, C. L. Manganelli, N. Zecevic, S. Faralli, G. Pares, R. Enne, A. Serrano, B. Goll, G. Fontana, A. Chalyan, J. M. Lee, P. Pintus, G. Chiaretti, H. Zimmermann, L. Pavesi, C. J. Oton, and S. Stracca, "Integrated reconfigurable silicon photonics switch matrix in IRIS project: Technological achievements and experimental results," *J. Light. Technol.* **37**, 345–355 (2019).
21. R. Amin, R. Maiti, Y. Gui, C. Suer, M. Miscuglio, E. Heidari, J. B. Khurgin, R. T. Chen, H. Dalir, and V. J. Sorger, "Heterogeneously integrated ITO plasmonic Mach–Zehnder interferometric modulator on SOI," *Sci. Rep.* **11**, 1–12 (2021).
22. J. Kim, S. Aghaeimeibodi, J. Carolan, D. Englund, and E. Waks, "Hybrid integration methods for on-chip quantum photonics," *Optica* **7**, 291–308 (2020).
23. F. Meinert, C. Hölzl, M. A. Nebioglu, A. D'Arnese, P. Karl, M. Dressel, and M. Scheffler, "Indium tin oxide films meet circular Rydberg atoms: Prospects for novel quantum simulation schemes," *Phys. Rev. Res.* **023192**, 1–7 (2020).
24. Y. Shen, N. C. Harris, S. Skirlo, M. Prabhu, T. Baehr-Jones, M. Hochberg, X. Sun, S. Zhao, H. Larochelle, D. Englund, and S. Marin, "Deep learning with coherent nanophotonic circuits," *Nat. Photonics* **11**, 441–446 (2017).
25. A. Forouzmand and H. Mosallaei, "Real-Time Controllable and Multifunctional Metasurfaces Utilizing Indium Tin Oxide Materials: A Phased Array Perspective," *IEEE Trans. Nanotechnol.* **16**, 296–306 (2017).
26. V. M. N. Passaro, F. Magno, and A. V. Tsarev, "Investigation of thermo-optic effect and multi-reflector tunable filter/multiplexer in SOI waveguides," *Opt. Express* **13**, 3429 (2005).
27. Q. Huang, K. S. Chiang, and W. Jin, "Thermo-optically controlled vertical waveguide directional couplers for mode-selective switching," *IEEE Photonics J.* **10**, 1–14 (2018).
28. P. Sun and R. M. Reano, "Submilliwatt thermo-optic switches using free- standing silicon-on-insulator strip waveguides," *Opt. Express* **18**, 1315–1320 (2010).
29. M. Jacques, A. Samani, E. El-Fiky, D. Patel, Z. Xing, and D. V. Plant, "Optimization of thermo-optic phase-shifter design and mitigation of thermal crosstalk on the SOI platform," *Opt. Express* **27**, 10456 (2019).
30. A. H. Atabaki, E. S. Hosseini, A. A. Eftekhar, S. Yegnanarayanan, and A. Adibi, "Optimization of metallic micro-heaters for reconfigurable silicon photonics," *Opt. Express* **18**, 18312–18323 (2010).
31. L. Yu, Y. Yin, Y. Shi, D. Dai, and S. He, "Thermally tunable silicon photonic microdisk resonator with transparent graphene nanoheaters," *Optica* **3**, 159 (2016).
32. Z. Xu, C. Qiu, Y. Yang, Q. Zhu, X. Jiang, Y. Zhang, W. Gao, and Y. Su, "Ultra-compact tunable silicon nanobeam cavity with an energy-efficient graphene micro-heater," *Opt. Express* **25**, 19479 (2017).
33. C. Ye, S. Khan, Z. R. Li, E. Simsek, and S. Member, "λ -Size

ITO and Graphene-Based Electro-Optic," *IEEE J. Sel. Top. Quantum Electron.* **20**, 3400310 (2014).
34. Z. Ma, Z. Li, K. Liu, C. Ye, and V. J. Sorger, "Indium-Tin-Oxide for High-performance Electro-optic Modulation," *Nanophotonics* **4**, 198–213 (2015).
35. R. Amin, C. Suer, Z. Ma, I. Sarpkaya, J. B. Khurgin, R. Agarwal, and V. J. Sorger, "Active material, optical mode and cavity impact on nanoscale electro-optic modulation performance," *Nanophotonics* **7**, 455–472 (2017).
36. G. Sinatkas and E. E. Kriezis, "Silicon-Photonic Electro-Optic Phase Modulators Integrating Transparent Conducting Oxides," *IEEE J. Quantum Electron.* **54**, 1 (2018).
37. Y. Gui, M. Miscuglio, Z. Ma, M. H. Tahersima, S. Sun, R. Amin, H. Dalir, and V. J. Sorger, "Towards integrated metatronics: a holistic approach on precise optical and electrical properties of Indium Tin Oxide," *Sci. Rep.* **9**, 1–10 (2019).
38. L. Caspani, R. P. M. Kaipurath, M. Clerici, M. Ferrera, T. Roger, J. Kim, N. Kinsey, M. Pietrzyk, A. Di Falco, V. M. Shalaev, A. Boltasseva, and D. Faccio, "Enhanced Nonlinear Refractive Index in ϵ -Near-Zero Materials," *Phys. Rev. Lett.* **116**, 1–5 (2016).
39. A. D. Neira, G. A. Wurtz, and A. V. Zayats, "All-optical switching in silicon photonic waveguides with an epsilon-near-zero resonant cavity [Invited]," *Photonics Res.* **6**, B1 (2018).
40. M. Z. Alam, I. De Leon, and R. W. Boyd, "Large optical nonlinearity of indium tin oxide in its epsilon-near-zero region," *Science* (80-.). (2016).
41. P. Guo, R. D. Schaller, L. E. Ocola, B. T. Diroll, J. B. Ketterson, and R. P. H. Chang, "Large optical nonlinearity of ITO nanorods for sub-picosecond all-optical modulation of the full-visible spectrum," *Nat. Commun.* **7**, 1–10 (2016).
42. S. Rajput, V. Kaushik, S. Jain, and M. Kumar, "Slow light enhanced phase shifter based on low-loss silicon-ITO hollow waveguide," *IEEE Photonics J.* **11**, 1–8 (2019).
43. R. Amin, R. Maiti, C. Carfano, Z. Ma, M. H. Tahersima, Y. Lilach, D. Ratnayake, H. Dalir, and V. J. Sorger, "0.52 v mm ITO-based Mach-Zehnder modulator in silicon photonics," *APL Photonics* **3**, 0–11 (2018).
44. J. Parra, J. Hurtado, A. Griol, and P. Sanchis, "Ultra-low loss hybrid ITO/Si thermo-optic phase shifter with optimized power consumption," *Opt. Express* **28**, 9393 (2020).
45. D. Chen, X. Xiao, L. Wang, Y. Yu, W. Liu, and Q. Yang, "Low-loss and fabrication tolerant silicon mode-order converters based on novel compact tapers," *Opt. Express* **23**, (2015).
46. M. Jacques, A. Samani, E. El-Fiky, D. Patel, Z. Xing, and D. V Plant, "Optimization of thermo-optic phase-shifter design and mitigation of thermal crosstalk on the SOI platform," *Opt. Express* **27**, 10456–10471 (2019).
47. R. B. Priti and O. Liboiron-Ladouceur, "Reconfigurable and Scalable Multimode Silicon Photonics Switch for Energy Efficient Mode-division-multiplexing Systems," *J. Light. Technol.* **37**, 3851–3860 (2019).
48. R. L. Espinola, M. C. Tsai, J. T. Yardley, and R. M. Osgood, "Fast and low-power thermooptic switch on thin silicon-on-insulator," *IEEE Photonics Technol. Lett.* **15**, 1366–1368 (2003).
49. K. Liu, C. Zhang, S. Mu, S. Wang, and V. J. Sorger, "Two-dimensional design and analysis of trench-coupler based Silicon Mach-Zehnder thermo-optic switch," *Opt. Express* **24**, 15845 (2016).
50. M. Totzeck, W. Ulrich, A. Göhnermeier, and W. Kaiser, "Semiconductor fabrication: Pushing deep ultraviolet lithography to its limits," *Nat. Photonics* **1**, 629–631 (2007).
51. M. Nedeljkovic, A. Z. Khokhar, Y. Hu, X. Chen, J. S. Penades, S. Stankovic, H. M. H. Chong, D. J. Thomson, F. Y. Gardes, G. T. Reed, and G. Z. Mashanovich, "Silicon photonic devices and platforms for the mid-infrared," *Opt. Mater. Express* **3**, 1205 (2013).
52. R. W. Johnson, A. Hultqvist, and S. F. Bent, "A brief review of atomic layer deposition: From fundamentals to applications," *Mater. Today* **17**, 236–246 (2014).
53. J. Schou, "Physical aspects of the pulsed laser deposition technique: The stoichiometric transfer of material from target to film," *Appl. Surf. Sci.* **255**, 5191–5198 (2009).
54. N. Riesen and J. D. Love, "Design of mode-sorting asymmetric Y-junctions," *Appl. Opt.* **51**, 2778–2783 (2012).
55. L. B. Soldano and E. C. M. Pennings, "Optical Multi-Mode Interference Devices Based on Self-Imaging: Principles and Applications," *J. Light. Technol.* **13**, 615–627 (1995).

VẬN DỤNG BỘ CHUYỂN PHA CÓ THỂ ĐIỀU KHIỂN DỰA TRÊN ÔXIT ITO ĐỂ THIẾT KẾ BỘ ĐỊNH TUYẾN CHỌN LỰA MODE QUANG BĂNG THÔNG CAO, NHỎ GỌN ĐƯỢC TÍCH HỢP TRÊN ỐNG DẪN SÓNG SOI

Tóm tắt: Gần đây, ITO, một oxít dẫn tốt, trong suốt và tương thích CMOS gây được sự chú ý mạnh mẽ trong công nghiệp quang tử silic điều khiển được bởi vì nó cho phép thu nhỏ khoảng cách giữa lõi silic và bộ gia nhiệt kim loại, do đó cho phép giảm tiêu thụ điện năng và tăng cường tốc độ chuyển mạch. Trong bài viết này, chúng tôi đề xuất một bộ gia nhiệt suy hao siêu thấp bằng ITO với kích thước nhỏ để điều chỉnh dịch pha nhiệt-quang. Bộ dịch pha có thể điều khiển sẽ được vận dụng để tạo ra một thiết kế số của một bộ định tuyến chọn lọc ba chế độ băng thông cao và nhỏ gọn. Kết quả mô phỏng băng thông 3 dB cho bộ định tuyến chọn lựa ba mode tương ứng là 100 nm và 40 nm với nhiễu xuyên âm dưới -25 dB. Bên cạnh đó, thiết bị được thiết kế đạt được dung sai chế tạo tương đối lớn tương ứng với dung sai chiều rộng và chiều cao là ± 50 nm và ± 5 nm. Ngoài ra, các thiết bị được đề xuất tiêu thụ tổng công suất tiêu thụ dưới 90 mW và thời gian chuyển đổi nhanh dưới 8 µs. Hơn nữa, cấu trúc thiết kế của bộ định tuyến được đề xuất có thể được tích hợp là 8 µm×2160 µm. Hiệu năng quang học tốt chứng tỏ tiềm năng hấp dẫn của ITO mở ra một nền tảng mới để tạo ra các hệ thống ghép kênh phân chia mode tốc độ cao cho mạch tích hợp quang tử kích thước rất lớn.

Từ khóa: oxít ITO; dịch pha quang nhiệt; nền tảng SOI; bộ định tuyến chọn lựa mode; thiết kế mô phỏng số;

Hang Duy Nguyen Thi was born in Quang Ninh province, Vietnam, in 1997. She received the B.E. degree from Posts and Telecommunications Institute of Technology (PTIT), Hanoi, in 2020, as an excellent degree. She is studying the master program. She is currently a teaching assistant at the PTIT institute. Her research interests include silicon photonic integrated circuits, optical high-speed communication systems, and deep learning development for communication.

Thanh Thuy Tran Thi was born in Hai Duong province, Vietnam, in 1998. She is currently a final-year student at the Posts and Telecommunications Institute of Technology (PTIT), Hanoi, as an excellent student. She is currently a teaching assistant at the PTIT institute. She is now studying the master program. Her research interests include photonic integrated circuits, silicon photonics, machine learning in photonic networks, all-optical signal processing, and optical high-speed communication systems.

Tan Hung Nguyen (S'08–M'12) was born in Danang, Vietnam, in 1980. He received the B.E. degree from the University of Danang-University of Science and Technology, Danang, in 2003, and the M.E. and Ph.D. degrees from the University of Electro-Communications, Tokyo, Japan, in 2009 and 2012, respectively. From 2012 to 2016, he was a Researcher with the National Institute of Advanced Industrial Science and Technology, Tsukuba, Japan, where he was involved in research on ultrafast and spectrally efficient all-optical signal processing, and development of an all-optical wavelength converter. He is currently a Teacher with the Department of Electronic and Telecommunication Engineering, The University of Danang-University of Science and Technology. He is also currently the Vice Dean of the Advanced Institute of The University of Danang. His research interests include high data capacity optical communication technologies. He is a member of the IEEE Photonics Society.

Cao Dung Truong was born in Thanh Hoa, Vietnam, in 1980. He received the B.E. degree and M.E. and Ph.D. degrees from Hanoi University of Science and Technology, Hanoi, in 2003, 2006 and 2015, respectively. He is currently a Teacher in the Department of Electronic Engineering, Posts and Telecommunications Institute of Technology, Hanoi, Vietnam. His research interests include photonic integrated circuits, plasmonics, photonic network-on-chip, AI for photonics and optical communication systems. He is currently a head of the AI-photonics lab at the PTIT institute.